Biosensors and Bioelectronics 42 (2013) 186–192

Contents lists available at SciVerse ScienceDirect

Biosensors and Bioelectronics

journal homepage: www.elsevier.com/locate/bios

Single-walled carbon nanotube field-effect transistors with graphene oxide passivation for fast, sensitive, and selective protein detection

Jingbo Chang [a], Shun Mao [a], Yang Zhang [a], Shumao Cui [a], Douglas A. Steeber [b], Junhong Chen [a,*]

[a] Department of Mechanical Engineering, University of Wisconsin-Milwaukee 3200 North Cramer Street Milwaukee, WI 53211, United States
[b] Department of Biological Sciences, University of Wisconsin-Milwaukee, 3209 North Maryland Ave Milwaukee, WI 53211, United States

ARTICLE INFO

Article history:
Received 17 July 2012
Received in revised form
24 September 2012
Accepted 10 October 2012
Available online 23 October 2012

Keywords:
Single-walled carbon nanotube
Graphene oxide
Au nanoparticle
Field-effect transistor
Biosensor
Passivation

ABSTRACT

We report a novel technique to design an insulating membrane with attachment sites on top of single-walled carbon nanotubes (SWNTs) for achieving high sensitivity and selectivity in an SWNT field-effect transistor (FET) biosensor. Because electronic properties of SWNTs are extremely sensitive to the surface state, direct immobilization of proteins or DNAs onto SWNTs will generate surface defects through chemical reactions or physical adsorption, resulting in degradation of performance and instability of SWNT-FET biosensor devices. Here we demonstrate fabrication of novel FET biosensor devices using SWNTs as semiconducting channels, and a monolayer of graphene oxide (GO) membrane covered on the SWNTs as a passivating layer to avoid direct attachment of biomaterials on SWNTs, thereby preserving intrinsic electrical properties of SWNTs. Gold nanoparticles (Au NPs) are decorated on the GO layer for the covalent attachment of biotin, which is then used to selectively detect the target avidin. The passivation with GO layers can effectively lead to enhanced sensitivity of biosensor devices through increasing the on/off ratio of FET sensors.

1. Introduction

Single-walled carbon nanotubes (SWNTs) have drawn significant attention for use in electronic applications due to their unique electrical, mechanical, and thermal properties (Lee et al., 2009). For instance, SWNTs configured as field-effect transistors (FETs) have been successfully used as nanoelectronic biosensors for detecting biomolecules. Dominant mechanisms for device responses include gating effects and Schottky barrier modification. Various biological interactions, such as DNA hybridization and antibody–antigen binding, have been monitored by measuring the conductance change of SWNT FETs (Allen et al., 2007; Kauffman and Star, 2008; Park et al., 2010; Sanchez-Acevedo et al., 2009; Vedala et al., 2011). The reliable detection of biological species using SWNT devices has proven attractive for label-free detection (Sorgenfrei et al., 2011) and real-time sensing (An et al., 2010; Kim et al., 2011), which is mainly attributed to the excellent sensitivity offered by SWNTs due to their ultra-sensitivity to electronic perturbations, large surface-to-volume ratio, outstanding signal-to-noise ratio (Heller et al., 2009), and high carrier mobility (Durkop et al., 2004).

Most current research on SWNT-based biosensors employs top-gate effects to detect DNAs or proteins through biomolecule immobilization on the SWNT surface using various noncovalent binding methods, such as physical adsorption (Chen et al., 2001; Maehashi et al., 2007; Star et al., 2003) through π stacking and hydrophobic interactions, or covalent binding methods (Khabashesku, 2011; Zhang et al., 2007), such as amidation and fluorination. However, it is well known that chemical species adsorbed on SWNTs will effectively "dope" SWNTs and modify their electronic properties because electrons move primarily along the SWNT surface (Xu et al., 2008). For example, even a single biomolecule (protein or DNA) attaching to the SWNT surface could effectively alter the electrical conductivity of the SWNT, because its size is comparable to the diameter of an SWNT (Chen et al., 2012). Therefore, direct immobilization of proteins onto SWNTs will degrade their electronic properties by generating defects through chemical or physical adsorption, which generally will lead to degradation of device performance and instability. For SWNT FET biosensors, it is a key technological challenge to control the surface states of SWNTs to achieve high sensitivity and selectivity.

One way to get around this issue is to design an insulating membrane with attachment sites on top of the active semiconductor channel, i.e., SWNTs, to capture target biomaterials. Here we demonstrate fabrication of novel FET biosensor devices using SWNTs as semiconducting channels, and a monolayer of graphene oxide (GO) membrane covered on the SWNTs as a passivating layer to avoid direct attachment of biomaterials on SWNTs, thereby preserving intrinsic electrical properties of SWNTs.

* Corresponding author.
E-mail address: jhchen@uwm.edu (J. Chen).

0956-5663/$ - see front matter © 2012 Elsevier B.V. All rights reserved.
http://dx.doi.org/10.1016/j.bios.2012.10.041

Gold nanoparticles (Au NPs) are decorated on the GO layer for the covalent attachment of biotin, which is then used to selectively detect the target avidin. The GO consists of a hexagonal ring-based carbon network having both sp^2-hybridized and sp^3-hybridized carbons with hydroxyl and epoxide functional groups on either side of the sheet. The extensive presence of saturated sp^3 bonds, the high density of electronegative oxygen atoms bonded to carbon (Boukhvalov and Katsnelson, 2008), and other "defects" give rise to an energy gap in the electron density of states to make GO non-conductive. GO sheets were selected as the passivation layer for the following reasons: (1) GO is an electrically insulating material with a high dielectric constant ($\kappa \approx 4.3$) (Standley et al., 2012) and does not directly interfere with the electron transport in the underlying carbon nanotubes; (2) GO sheets are water-soluble and can be easily processed for patterning; (3) a monolayer GO sheet is ~0.8 nm in thickness and can be used to readily obtain the desired number of layers through controlled deposition; (4) GO has a relatively high Young's modulus ($E_{GO}=207$ GPa (Suk et al., 2010)), which can induce large compressive loads on the underlying nanotubes. In the case of SWNT FET biosensor devices, proposed mechanisms include charge-induced electrostatic gating, capacitance modulation, Schottky barrier effect, and carrier mobility change. In our case, the novel device with a GO passivation layer will be mainly operated through the top-gating effect, an isolated sensing mechanism that simplifies understanding of the sensing platform. Our work contributes directly to the study of engineering passivation layers on SWNT FETs and presents a promising route for improving electronic properties of FETs for high-performance biosensor applications.

2. Materials and methods

2.1. Materials

SWNTs (~98% semiconducting) were ordered from NanoIntegris, which were synthesized using the chemical vapor deposition (CVD) method. 2-aminoethanethiol (AET), dimethyl sulfoxide (DMSO), avidin, and biotin N-hydroxysuccinimide ester (biotin-NHS) were purchased from Sigma-Aldrich. Tween 20 and cold water fish gelatin were ordered from Tedpella; bovine serum albumin (BSA) was purchased from Rockland. PBS (pH 7.4, ×1) (Fisher BioReagents) was used as the solvent for avidin, biotin and blocking buffer. All solutions were prepared with deionized (DI) water (Cellgro).

2.2. Device fabrication

SWNT FETs were fabricated by drop-casting the SWNT suspension on Au interdigitated electrodes. Au electrodes with both finger-width and inter-finger spacing (source and drain separation) of about 1 μm and a thickness of 50 nm were fabricated using an e-beam lithography process (Raith 150 lithography tool, 30 kV) on a highly doped Si wafer with a top layer of dry formed SiO_2 (thickness of 200 nm) (Mao et al., 2010). The device was annealed in argon flow (1 standard cubic centimeters per minute) for one hour at 300 °C to improve the contact quality and reduce the junction barriers between Au electrodes and SWNTs. GO sheets were produced from natural graphite powder using the modified Hummers method reported previously (Mao et al., 2011). The synthesized GO sheets were dispersed in a mixture of DI water and methanol (1:5, v/v) and deposited onto the SWNT device by a solution shrinkage method. The deposition of Au NPs onto SWNT/GO device was carried out using an RF (60 Hz) Emitech K550x Sputter coater apparatus with Au source (99.999% purity target) at Ar pressure of 0.03 mbar. The deposition time was 2 s with a working current of 10 mA, leading to Au NPs with a size of 2.5 nm. The sensing experiments were performed with a poly(dimethylsiloxane) window covered on the devices, resulting in encapsulated electrodes (source and drain) and an open-sensing area, where solution-access was restricted to the exposed region only.

2.3. Immobilization

2-Aminoethanethiol (AET, 1 mg/ml) in DI water at a concentration of 10 mM was immobilized on the device with Au NP as a linker to conjugate with biotin-NHS. Biotinylated surfaces were obtained by reaction with biotin-NHS (200 μg/ml) in a mixture of DMSO/buffer for 1 h. Devices were incubated with the blocking buffer (0.1% tween 20, 0.1% fish gelatin, and 1% BSA) for 1 h at room temperature and then washed with the PBS buffer.

2.4. Characterization

Electrical measurements were performed on SWNT/GO/Au NPs biosensors using a Keithley 4200 semiconductor characterization system. Three-terminal FET measurements were employed for device transport characteristics; other electrical tests were performed using two-terminal measurements with a floating gate. The electrical conductance of the biosensor was measured by fixing the drain voltage (V_{SD}) and simultaneously recording the drain current (I_{SD}) when the device was exposed to different concentrations of target biomaterials.

3. Results and discussion

The method to introduce attachment sites on the SWNT FET devices without direct modification of SWNTs will provide significant advantages for detecting biological species. A schematic of the device fabrication process is illustrated in Fig. 1. Individual semiconducting SWNTs were deposited across a pair of gold electrodes shown in Fig. 1a using a drop-casting process, causing SWNTs to act as the conducting channel materials in the FET sensor. Charge carrier mobility (μ) and on/off ratio are highly sensitive to the surface status of SWNTs in the channel; therefore, protection layers (GO sheets) are necessary for optimizing SWNT FET performance, as shown in Fig. 1b. Au NPs are readily functionalizable and have been reported to have the highest affinity for thiol groups, resulting in viable analyte-binding sites (Love et al., 2005); therefore, Au NPs were employed to deposit onto the GO layers as scaffolds with the conjugation of thiol ligands to capture target biomaterials in Fig. 1c. Fig. 1d shows that 2-aminoethanethiol (AET), which contains amine and thiol functional end groups, chemically bonds to Au NPs through Au-thiol interactions. To capture target proteins (avidin), biotin N-hydroxysuccinimide ester (biotin-NHS) was conjugated with amine groups of AET. Blocking buffer agents were used to prevent the non-specific binding of avidin. During the sensing test, binding events induced significant changes in the FET electrical characteristics after introducing avidin, which were monitored by a Keithley 4200 Semiconductor Characterization Systems.

The biosensor device was constructed by decorating GO-covered SWNTs with Au nanoparticles on the Au electrodes. Fig. 2a shows scanning electron microscopy (SEM) images of individual SWNTs with a diameter of 1 nm and a length of about 2 μm across a pair of 1 μm-apart Au electrodes. The SWNT areal density in each device was estimated at approximately 2 tubes per μm^2 by fixing the concentration (1 mg/100 ml) and the volume (1 μm) of the SWNT suspension used for drop-casting. To control the electronic stability of devices, metallic SWNTs were burnt off by ramping the drain-source voltage under the

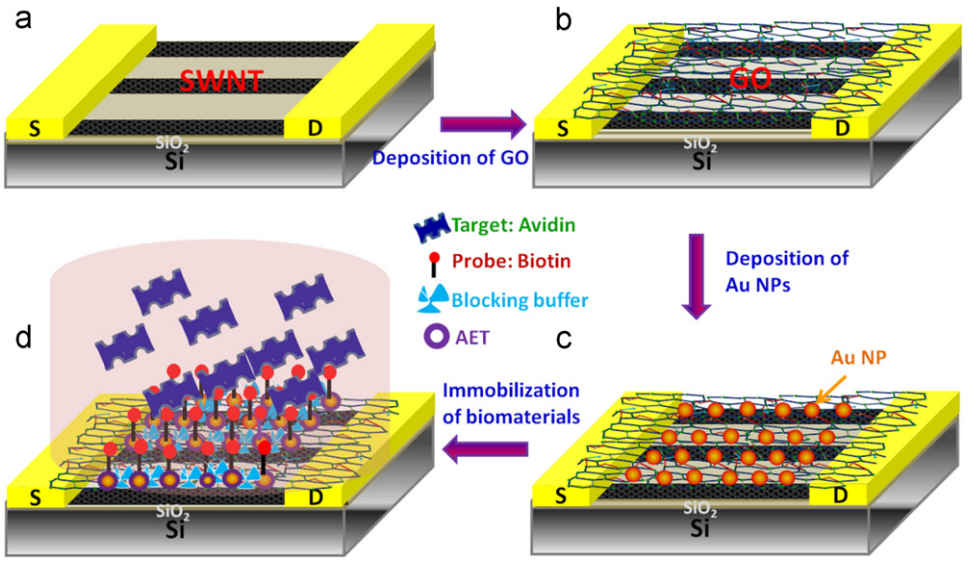

Fig. 1. Schematic illustration of the SWNT/GO FET biosensor fabrication process. (a) SWNTs were deposited across the Au electrode gap, (b) A GO membrane covered on SWNTs, (c) Deposition of Au NPs on the GO membrane, and (d) Attachment of probe biotins on Au NPs through covalent bonding for capturing target avidins.

insulating (off) state of semiconducting nanotubes. SWNTs have the smallest diameters among various one-dimensional structured materials, which are composed entirely of surface atoms in direct contact with attached species. The electronic properties of SWNTs are extremely sensitive to the surface state and the environment; therefore, use of protection layers for SWNTs (Wongwiriyapan et al., 2011) can potentially lead to optimized SWNT sensor performance. Engineering GO membranes onto SWNTs was accomplished by using a facile solution-phase deposition approach (Fig. S1, Supporting Information), which is suitable for large-scale processing and integration. The structural morphology of GO membranes covered on top of nanotubes is shown in Fig. 2b, in which the GO edge is outlined using red dashed lines and an SWNT is highlighted using a blue dashed line. Because the 0.8 nm-thick (Fig. S2, Supporting Information) monolayer GO is transparent, SWNTs are clearly seen underneath the GO layer as evidenced by the SEM image shown in Fig. 2b. Zheng et al. (Zheng et al., 2012) measured the binding/adhesion energy between monolayer GO sheets and SiO_2/Si substrates as 0.038 J/m^2, which is strong enough to fix GO sheets on the device. The uniformity of GO coverage on Si wafers and sensor devices has been investigated (Fig. S3, Supporting Information), which showed that more than 95% of the device surface area was covered with GO membranes. Because GO sheets have irregular shapes, it is difficult to produce perfect monolayer GO membranes; however, close-packed membranes are not critical for the current application. In fact, the as-produced GO membranes significantly enhanced semiconducting properties of the SWNT FET devices.

Au NPs were specifically chosen for this biosensor application due to their versatility in conjugating analyte molecules through thiolated capturing probes. An ordered array of individual particles on the surface is needed for optimum detection with NPs (Schwartz and Quakea, 2007), because it will allow for a higher areal density and more uniform distribution of attachment sites conducive for sensitive and reproducible sensors. Conventional patterning of NPs is accomplished through various expensive patterning techniques (e.g., lithography, microcontact printing, or direct surface patterning) (Ibanez and Zamborini, 2012). In this work, fabrication of Au NPs at a high areal density was achieved by using a simple sputtering deposition method. NPs with sizes of approximately 2.5 nm and inter-particle spacing of about 3 nm are uniformly deposited on the GO membrane, as shown in Fig. 2c and d (a higher magnification). Transmission electron microscopy (TEM) and high-resolution TEM (HRTEM) images in Fig. 2e and f also clearly show that individual and discrete Au NPs are uniformly distributed on the GO membrane. The ability to tune the distance between the attachment sites is important. If Au NPs form a continuous film, the resulting metallic film will screen any effects induced by charged target biomaterials in the device; therefore, engineering the NP center-to-center spacing is crucial to allow for a higher NP areal density with no aggregation. In this study, the Au NP size and inter-particle spacing can be adjusted by controlling the deposition time (Fig. S5, Supporting Information).

We investigated the effect of Au NPs (~2.5 nm) decoration on the electrical properties of SWNT-FETs with and without the GO membrane protection. Fig. 3a shows the current-gate voltage characteristics (source-drain current I_{SD} vs. gate voltage V_G) of the SWNT-FETs without GO membranes before (black) and after (blue) decoration of Au NPs. The device shows clear p-type semiconducting behavior with an on/off ratio=253 and a complete depletion of the current around a threshold voltage $V_{th}=-20$ V. However, the SWNT-FET was found to have lost much of its gate dependence after coating SWNTs with Au NPs, which reduced the on/off ratio to an extremely low value of ~1.18 and the overall conductance of the device decreased substantially. The loss of gate dependence could be ascribed to the scattering and doping effects from Au NPs (Kim et al., 2006). We also observed hysteresis effects that are commonly seen in SWNTs and graphene FETs, which are mainly attributed to the charge transfer between the CNT and charge traps at the silicon oxide/ambient interface (Franklin et al., 2012; Ganzhorn et al., 2011). When GO membranes covered the SWNTs, the on/off ratio increased to a much larger value than that of bare SWNT devices (Fig. 3b). The GO showed great promise for use as a layered dielectric, particularly because it is graphene's native oxide. Similar to SWNT devices, the conductance of the GO-passivated device decreased after Au NPs decoration and the on/off ratio became much smaller; however, the SWNT/GO/Au NP device still showed much better semiconducting behavior than the SWNT/Au NP device (without GO passivation).

In SWNT-Au NP heterojunction systems, charge redistribution at the SWNT-NP interface takes place due to Fermi level alignment. Since the Au work function (5.1 eV) is larger than that of the SWNT (5.0 eV), electrons transfer from the SWNT to the Au NPs.

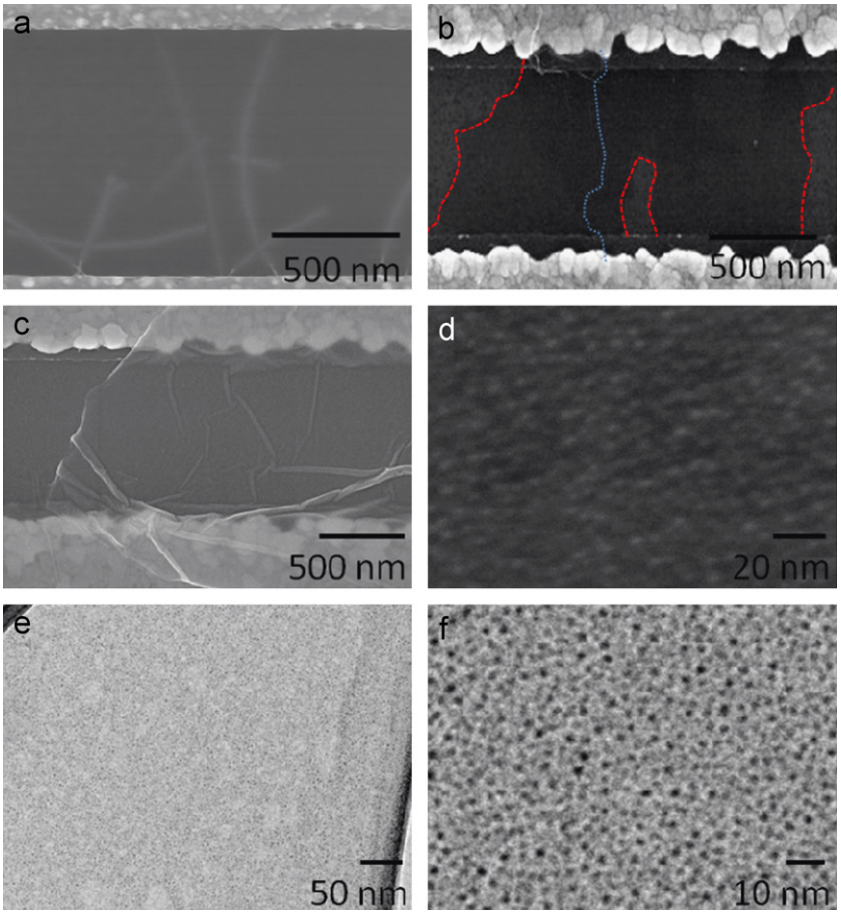

Fig. 2. SEM images of (a) SWNTs bridging an Au electrode gap, (b) GO membranes covering the device, with an underlying SWNT highlighted using a blue dashed line and GO sheets outlined using red dashed lines, (c) Au NPs coating the GO membrane, and (d) high-magnification isolated Au NPs on the GO membrane; (e) and (f) TEM images of Au NP distribution on the GO membrane. (For interpretation of the references to color in this figure legend, the reader is referred to the web version of this article.)

The electron donation from SWNTs to Au NPs leads to a decrease in the SWNT Fermi level, resulting in the upward band bending of the valence and conduction band edges as shown in Fig. 3c. As a result, a hole accumulation region forms near the interface, as schematically shown in the upper panel of Fig. 3d, giving rise to scattering and thus a decrease in the hole mobility. The GO coverage could alleviate the accumulation of holes and hence the scattering effect at the SWNT/Au NP interface, probably owing to GO's insulating properties, as illustrated in the lower panel of Fig. 3d. The on-state source-drain current increased significantly after depositing GO membranes on the SWNTs, as shown in Fig. 3b (red line). The increase in current might be understood as follows. The source-drain current can be expressed as (Sze and Ng, 2007),

$$I_{SD} = \mu C_{tube} \frac{W}{L}\left[(V_G - V_{th})V_{SD} - \frac{V_{SD}^2}{2}\right] \quad (1)$$

where μ is carrier mobility, C_{tube} is the capacitance of SWNTs, W and L are the channel width and length, respectively. The capacitance C_{tube} can be represented by (Martel et al., 1998),

$$C_{tube} = \frac{2\pi\varepsilon_0\varepsilon_r}{\ln(2t/r)} \quad (2)$$

where ε_0 is the vacuum permittivity, ε_r is the average relative permittivity surrounding a tube, t is the thickness of the backside gate oxide, and r is the tube radius. The GO coverage on SWNTs effectively increases the relative permittivity ε_r surrounding the tube, because GO has a relative permittivity of ~4.3 (Standley et al., 2012), which is much larger than that of air (~1). Therefore, the tube capacitance C_{tube} increased after the GO passivation according to Eq. (2). Consequently, the source-drain current increased provided that other parameters in Eq. (1) were fixed. Another possible reason for the increase of I_{SD} is that more effective gating was achieved due to the buckling effect of GO coverage, which resulted in a stronger attachment of SWNTs on the SiO_2 substrate. The degradation of source-drain current after deposition of Au NPs on the GO membranes (blue curve in Fig. 3b) could still be attributed to the scattering effect caused by the slight hole accumulation at the SWNT/Au NP interface, because the GO membranes (~0.8 nm) were not thick and insulating enough to prevent the charge transfer between Au NPs and SWNTs. In order to improve the stability and the repeatability of the device in the future work, it is important to develop methods to better control the quality of deposition of GO layers such as coverage fraction, the number of layers, and selected-area deposition (Yang et al., 2012).

The sensing performance of SWNT/GO/Au NP devices was investigated using avidin as a model analyte. Because the interaction between biotin and avidin has the highest known ligand–protein affinity, the biotin–avidin system is widely used in many biotechnological applications such as markers for proteins and nucleic acids. As the isoelectric point (pI) of avidin (10.5) is higher than the pH value (7.4) of phosphate buffered saline (PBS) buffer, avidin proteins carry positive charges in PBS. According to the gating effect of a p-type SWNT FET, it is anticipated that positively charged avidin proteins will result in a decrease in the current during the sensing operation. In our experiments, the pH of PBS was kept constant (7.4). By changing the pH of the avidin solution, the charges on avidin will change, resulting in variations in the

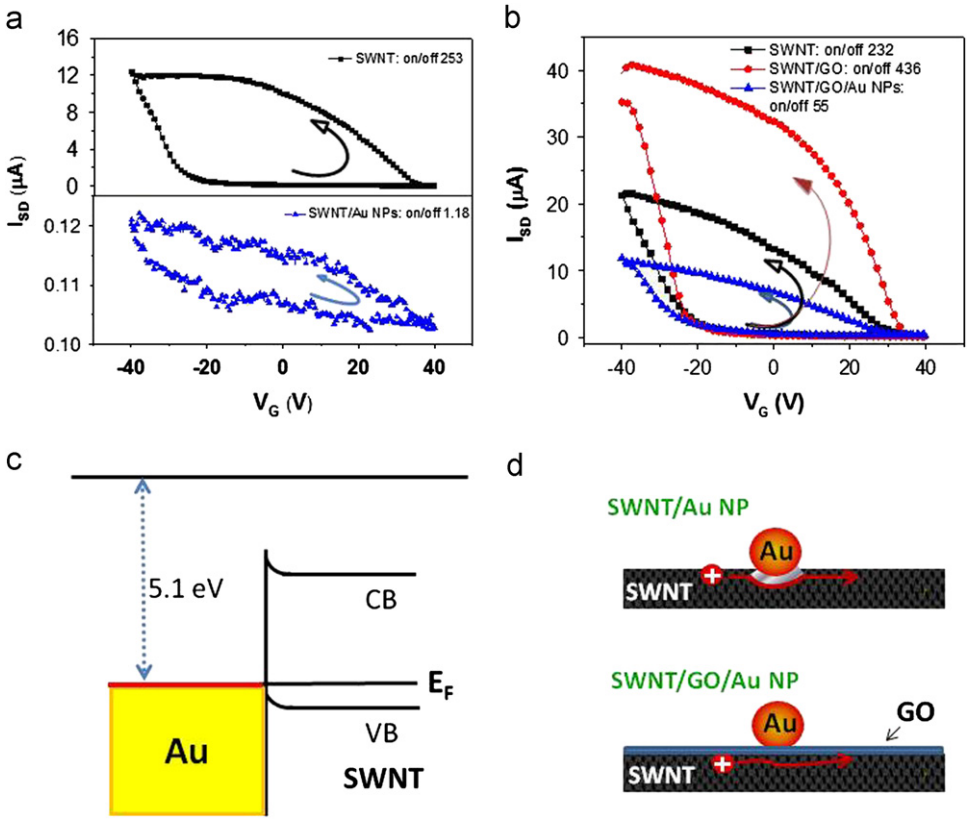

Fig. 3. (a) Drain current (I_{SD}) vs. back gate voltage (V_G) for bare SWNTs (black) and SWNTs with Au NPs (2.5 nm) decoration (blue). (b) I_{SD} vs. V_G for bare SWNTs (black), SWNTs with GO membranes (red), and SWNTs covered with GO coated with Au NPs (2.5 nm) (blue). Source-drain voltage is 100 mV for each case, and sweeping directions are indicated by the arrows. (c) Band diagram for Au NPs-decorated SWNTs. (d) Au NP decoration on the SWNT results in a localized depletion region indicated by a white area (upper panel) and a GO membrane works as an insulating layer to avoid direct interactions between an SWNT and an Au NP (lower panel). (Work function of Au=5.1 eV, work function of SWNT=5.0 eV). (For interpretation of the references to color in this figure legend, the reader is referred to the web version of this article.)

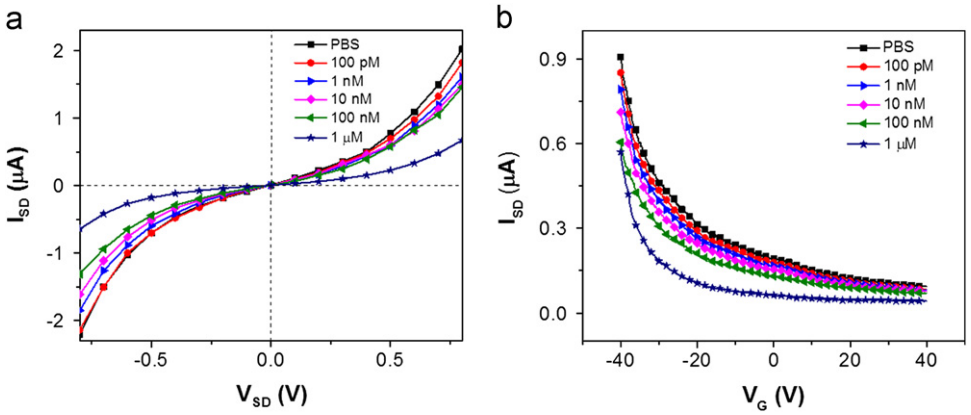

Fig. 4. Avidin detection through electrical measurements: (a) Source-drain voltage dependence (V_G=0 V) of the drain current I_{SD} and (b) typical gate voltage dependence (V_{SD}=0.1 V) of the drain current I_{SD} upon the introduction of avidin with different concentrations. The experiments were carried out in PBS (pH 7.4, ×1).

sensor current. To investigate the sensitivity of the biosensor, the device was exposed to varying concentrations of avidin in the PBS buffer. Fig. 4a illustrates the drain-source voltage dependence of the drain current I_{SD} of our sensor after adding selected concentrations of avidin (10^{-10}, 10^{-9}, 10^{-8}, 10^{-7}, 10^{-6} and 10^{-5} M) dissolved in PBS buffer. It can be observed that the conductance of the devices continued to decrease with increasing concentrations of avidin. The source-drain voltage (V_{SD}) dependence of I_{SD} of the devices was slightly non-linear likely due to charge injection during measurements. We also investigated changes in transfer curves of the FET sensor with different avidin concentrations (Fig. 4b), which is consistent with the source-drain voltage dependence where a binding event between avidin and biotin led to a decrease in the conductivity of SWNT/GO devices.

Fig. 5a and b show the dynamic response of SWNT-based devices with and without GO passivation, respectively. The conductance of the device with GO membranes decreased correspondingly with the addition of avidin, and the current change of the device was around 8.6% with the introduction of 100 pM avidin. For comparison, a control experiment was carried out on a device without GO membranes. Based on the results shown in Fig. 5b, the sensor conductance decreased upon specific binding

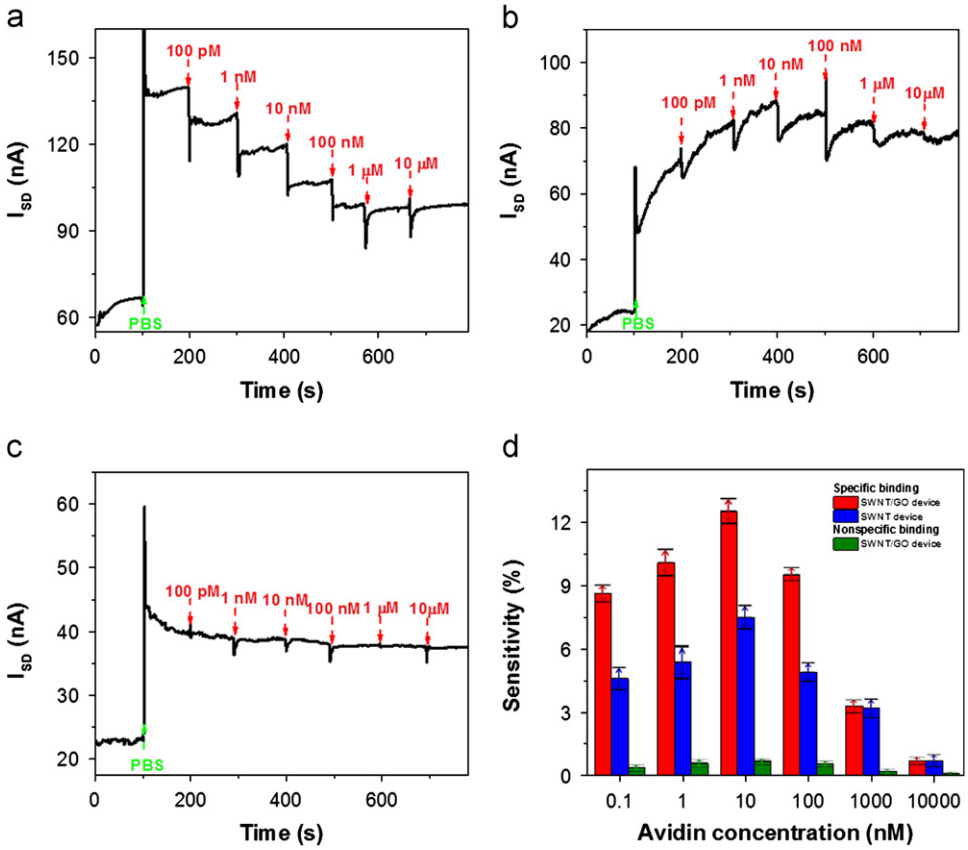

Fig. 5. Dynamic response of the devices exposed to different concentrations of avidin for (a) specific binding in the SWNT/GO FET device, (b) specific binding in SWNT FET device (without GO passivation), and (c) non-specific binding in the SWNT/GO FET device (without biotin probes); (d) Sensor sensitivity vs. avidin concentration. Error bars were obtained through multiple measurements. For all measurements, V_{SD}=0.1 V and V_G=0 V. The experiments were carried out in PBS (pH 7.4, ×1).

between biotin and avidin at different concentrations; however, the SWNT device without GO coverage showed a much smaller decrease in current (4.6%) with the addition of 100 pM avidin and a corresponding smaller response to each increasing concentration of avidin up to 10 μM. Furthermore, the SWNT/GO/Au NP devices show better sensing properties than that of SWNT/Au NP devices, such as a faster response and less conductivity drift. This is possibly due to the higher thermal conductivity of SWNT/GO for efficient device cooling as well as minimization of non-specific binding events with the GO membrane passivation on the SWNTs. In contrast, controlled injection of avidin had almost no effect on the conductance of the SWNT/GO/Au NP devices without the presence of biotin probes (Fig. 5c). Therefore, it is confirmed that the conductance drops are solely attributed to the specific binding between probe and target proteins.

A summary of the sensor sensitivity (relative resistance change, %) is presented in Fig. 5d for different avidin concentrations. The SWNT/GO/Au NP devices show a higher sensitivity response to each avidin concentration than that of the SWNT/Au NP devices. Both sensors show a non-linearly increased response with the introduction of avidin at concentrations from 0.1 to 10 nM, which further suggests sensor responses come from binding avidin to biotin, and the response amplitude depends on the avidin concentration. With more avidins binding to biotins on the devices, a larger gating effect will be introduced and more significant carrier mobility change will result, thereby leading to more pronounced conductivity change in the sensor. When the avidin concentration reached 10 nM, the sensor response became saturated, and further increase in the avidin concentration led to only slight changes in the sensor resistance. This phenomenon indicates that at 10 nM concentration level most of the binding sites on the devices are occupied by target proteins. For non-specific binding without the presence of biotin probes, the SWNT/GO/Au NP device showed only a very weak response because the blocking buffer and GO (Nair et al., 2012) can effectively block physical adsorption of avidin on the device. Without the GO passivation layer on the SWNTs, the device also detected avidin, but the sensitivity was much smaller, indicating that the passivation by the GO layer is very effective at protecting electrical properties of SWNTs. The substantially increased sensitivity is primarily due to the GO passivation layer, the immobilization of a relatively larger number of proteins, and the higher on/off ratio of the FET device.

Understanding the effect of SWNT electrical properties on the sensor performance will lead to better designs of nanotube biosensors and more reliable fabrication procedures. Recently, Fu et al. reported (Fu et al., 2010) that the on/off ratios of SWNT network devices could be tuned simply by changing the percentage of semiconducting SWNTs or by changing the tube density in the network to obtain a high sensitivity biosensor. Furthermore, Ishikawa et al. (Ishikawa et al., 2010) demonstrated that controlling nanotube density in order to minimize direct metallic nanotube pathways was critical in achieving high/reliable performance of FET biosensors. In fact, both of these groups have improved biosensor performance due to the enhancement of SWNT semiconducting properties (on/off ratio, charge mobility, and elimination of metallic nanotube pathways). In general, device fabrication and operation processes, such as surface modification of SWNTs, immobilization of biomaterials, and liquid phase detection environment, could degrade the performance of biosensor devices. Therefore, the GO sheet is a promising candidate for passivation with atomic layer thickness,

easy processing due to water solubility, and desired dielectric properties.

The mechanism for such a device conductivity change is likely the direct electrostatic gating effect from accumulation of positively charged avidin. In our experiments, 1 × PBS was used with a predicted Debye length of about ~0.7 nm (Stern et al., 2007). In reality the Debye length might be significantly larger than 0.7 nm due to the source-drain bias or electrostatic potential change induced by the positively charged avidin (Stern et al., 2007). Of course, some of the avidin proteins could link to the side/bottom surface of these isolated Au NPs and the distance between the avidin and SWNTs could be as small as 0.8 nm (thickness of the GO layer). Besides the gating effect, a potential issue for the design of reliable SWNT biosensor devices is that proteins could also adsorb at the Schottky contact between SWNTs and Au electrodes and lead to a significant but non-specific conductance change due to work function modulation of Au electrodes. With the passivation layers of GO membranes, charge transfer between biomaterials and electrodes could be minimized. The reported biosensor performance could be further improved by optimizing SWNT/GO/Au NP devices, such as through the control of GO nanosheet thickness, uniformity of GO membranes, and the number of GO layers. For instance, Javey et al. (Javey et al., 2002) used high dielectric constant ZrO_2 to construct SWNT logic gates, which greatly improved device performance. GO has a slightly high dielectric constant ($\kappa \approx 4.3$), thereby allowing for efficient charge injection into transistor channels while reducing direct tunneling leakage currents, resulting in high FET performance (Osada and Sasaki, 2012). GO can be used to not only protect the SWNT surface from generating more defects during the integration of SWNTs into biosensor devices, but also avoid non-specific binding like a blocking agent. The intrinsic electrical properties of semiconducting SWNTs combined with advanced gate dielectrics (GO sheets) may open a new route to design high-performance SWNT FET biosensor devices.

4. Conclusions

In this paper, our study suggested the importance of considering the surface state of SWNTs when designing a carbon nanotube-based FET biosensor. To minimize modification of SWNT surface states, such as surface modification and immobilizing biomaterials on the SWNTs, and the subsequent degradation of device performance, we have demonstrated a method to protect electrical properties of SWNTs by using dielectric GO sheets. The passivation with GO layers can effectively lead to enhanced sensitivity of biosensor devices through increasing the on/off ratio of FET sensors. The performance of SWNT FET biosensor devices can be further improved through controlling the number, uniformity, and coverage of GO to form an ultra-thin insulating layer.

Acknowledgments

Financial support for this work was provided by the US National Science Foundation (CMMI-0900509) and University of Wisconsin-Milwaukee Research Foundation Bradley Catalyst Grant. The e-beam lithography was performed at the Center for Nanoscale Materials of Argonne National Laboratory, which is supported by the US Department of Energy, Office of Science, Office of Basic Energy Sciences, under Contract no. DE-AC02-06CH11357. The authors thank Dr. H.A. Owen for technical support with SEM analyses, and Dr. S.E. Hardcastle with AFM analysis.

Appendix A. Supporting information

Supplementary data associated with this article can be found in the online version at http://dx.doi.org/10.1016/j.bios.2012.10.041.

References

Allen, B.L., Kichambare, P.D., Star, A., 2007. Advanced Materials (Weinheim, Germany) 19 (11), 1439–1451.
An, T., Kim, K.S., Hahn, S.K., Lim, G., 2010. Lab on a Chip 10 (16), 2052–2056.
Boukhvalov, D.W., Katsnelson, M.I., 2008. Journal of the American Chemical Society 130 (32), 10697–10701.
Chen, R.J., Zhang, Y.G., Wang, D.W., Dai, H.J., 2001. Journal of the American Chemical Society 123 (16), 3838–3839.
Chen, Y.N., Vedala, H., Kotchey, G.P., Audfray, A., Cecioni, S., Imberty, A., Vidal, S., Star, A., 2012. ACS Nano 6 (1), 760–770.
Durkop, T., Getty, S.A., Cobas, E., Fuhrer, M.S., 2004. Nano Letters 4 (1), 35–39.
Franklin, A.D., Tulevski, G.S., Han, S.J., Shahrjerdi, D., Cao, Q., Chen, H.Y., Wong, H.S.P., Haensch, W., 2012. ACS Nano 6 (2), 1109–1115.
Fu, D., Okimoto, H., Lee, C.W., Takenobu, T., Iwasa, Y., Kataura, H., Li, L.-J., 2010. Advanced Materials (Weinheim, Germany) 22 (43), 4867–4871.
Ganzhorn, M., Vijayaraghavan, A., Green, A.A., Dehm, S., Voigt, A., Rapp, M., Hersam, M.C., Krupke, R., 2011. Advanced Materials (Weinheim, Germany) 23 (15), 1734–1738.
Heller, I., Mannik, J., Lemay, S.G., Dekker, C., 2009. Nano Letters 9 (1), 377–382.
Ibanez, F.J., Zamborini, F.P., 2012. Small (Weinheim an der Bergstrasse, Germany) 8 (2), 174–202.
Ishikawa, F.N., Curreli, M., Olson, C.A., Liao, H.I., Sun, R., Roberts, R.W., Cote, R.J., Thompson, M.E., Zhou, C.W., ACS Nano 4 (11), 6914–6922.
Javey, A., Kim, H., Brink, M., Wang, Q., Ural, A., Guo, J., McIntyre, P., McEuen, P., Lundstrom, M., Dai, H.J., 2002. Nature Materials 1 (4), 241–246.
Kauffman, D.R., Star, A., 2008. Chemical Society Reviews 37 (6), 1197–1206.
Khabashesku, V.N., 2011. Russian Chemical Reviews 80 (8), 705–725.
Kim, B.K., Park, N., Na, P.S., So, H.M., Kim, J.J., Kim, H., Kong, K.J., Chang, H., Ryu, B.H., Choi, Y.M., Lee, J.O., 2006. Nanotechnology 17 (2), 496–500.
Kim, J.P., Hong, S., Sim, S.J., 2011. Journal Nanoscience Nanotechnology 11 (5), 4182–4187.
Lee, J., Liao, A., Pop, E., King, W.P., 2009. Nano Letters 9 (4), 1356–1361.
Love, J.C., Estroff, L.A., Kriebel, J.K., Nuzzo, R.G., Whitesides, G.M., 2005. Chemical Reviews 105 (4), 1103–1169.
Maehashi, K., Katsura, T., Kerman, K., Takamura, Y., Matsumoto, K., Tamiya, E., 2007. Analytical Chemistry 79 (2), 782–787.
Mao, S., Lu, G.H., Yu, K.H., Bo, Z., Chen, J.H., 2010. Advanced Materials. 3521.
Mao, S., Yu, K.H., Cui, S.M., Bo, Z., Lu, G.H., Chen, J.H., 2011. Nanoscale 3 (7), 2849–2853.
Martel, R., Schmidt, T., Shea, H.R., Hertel, T., Avouris, P., 1998. Applied Physics Letters 73 (17), 2447–2449.
Nair, R.R., Wu, H.A., Jayaram, P.N., Grigorieva, I.V., Geim, A.K., 2012. Science 335 (6067), 442–444.
Osada, M., Sasaki, T., 2012. Advanced Materials 24 (2), 210–228.
Park, M., Cella, L.N., Chen, W.F., Myung, N.V., Mulchandani, A., 2010. Biosenors and Bioelectronics 26 (4), 1297–1301.
Sanchez-Acevedo, Z.C., Riu, J., Rius, F.X., 2009. Biosensors and Bioelectronics 24 (9), 2842–2846.
Schwartz, J.J., Quakea, S.R., 2007. Applied Physics Letters 91, 8.
Sorgenfrei, S., Chiu, C.Y., Gonzalez, R.L., Yu, Y.J., Kim, P., Nuckolls, C., Shepard, K.L., 2011. Nature Nanotechnolgy 6 (2), 125–131.
Standley, B., Mendez, A., Schmidgall, E., Bockrath, M., 2012. Nano Letters 12 (3), 1165–1169.
Star, A., Gabriel, J.C.P., Bradley, K., Gruner, G., 2003. Nano Letters 3 (4), 459–463.
Stern, E., Wagner, R., Sigworth, F.J., Breaker, R., Fahmy, T.M., Reed, M.A., 2007. Nano Letters 7 (11), 3405–3409.
Suk, J.W., Piner, R.D., An, J.H., Ruoff, R.S., 2010. ACS Nano 4 (11), 6557–6564.
Sze, S.M., Ng, K.K., 2007. Physics of Semiconductor Devices, 3rd ed. Wiley-Interscience, Hoboken, N.J.
Vedala, H., Chen, Y.A., Cecioni, S., Imberty, A., Vidal, S., Star, A., 2011. Nano Letters 11 (1), 170–175.
Wongwiriyapan, W., Okabayashi, Y., Minami, S., Itabashi, K., Ueda, T., Shimazaki, R., Ito, T., Oura, K., Honda, S., Tabata, H., Katayama, M., 2011. Nanotechnology 22, 5.
Xu, N., Ding, J.W., Xing, D.Y., 2008. Journal Applied Physics 103, 8.
Yang, J., Kim, J.-W., Shin, H.S., 2012. Advanced Materials 24 (17), 2299–2303.
Zhang, Y.B., Kanungo, M., Ho, A.J., Freimuth, P., van der Lelie, D., Chen, M., Khamis, S.M., Datta, S.S., Johnson, A.T.C., Misewich, J.A., Wong, S.S., 2007. Nano Letters 7 (10), 3086–3091.
Zheng, M., Zou, L.F., Wang, H., Park, C., Ke, C.H., 2012. ACS Nano 6 (2), 1814–1822.